



# Contrasting intensity of aragonite dissolution and dolomite cementation in glacial versus interglacial intervals of a subtropical carbonate succession

LARS REUNING\* , HANAA DEIK†, BENJAMIN PETRICK\*, GERALD AUER‡, HIDEKO TAKAYANAGI§, YASUFUMI IRYU§ , MARGOT COURTILLAT¶ and MARIA-ANGELA BASSETTI¶

\*Institute of Geosciences, CAU Kiel University, Ludewig-Meyn-Straße 10, Kiel 24118, Germany (E-mail: lars.reuning@ifg.uni-kiel.de)

†Geological Institute, RWTH Aachen University, Wüllnerstrasse 2, Aachen, 52062 Germany

‡Institute of Earth Sciences (Geology and Paleontology), NAWI Graz Geocenter, University of Graz, Heinrichstraße 26, Graz, 8010 Austria

§Institute of Geology and Paleontology, Tohoku University, Aobayama, Sendai, 980-8578 Japan

¶Centre de Formation et de Recherche sur les Environnements Méditerranéens, Université de Perpignan Via Domitia, UMR 5110, CEDEX, 52 Avenue Paul Alduy, Perpignan, F-66860 France

Associate Editor – Nicholas Tosca

## ABSTRACT

Aragonite and high-Mg calcite are abundant in modern, neritic carbonate systems but almost absent in their fossil counterparts. Dissolution of these metastable mineral phases commonly leaves no visible trace in the sedimentary record, compromising the derivation of palaeoenvironmental information from the rock record. The upper 25 m of Integrated Ocean Drilling Program (IODP) Site U1460 on the outer ramp of the western Australian Shelf were investigated to study shallow burial (tens of metres) marine diagenesis in organic-carbon poor sediments using microscopic, total organic carbon, biomarkers and mineralogical analysis in combination with pore-water geochemistry. Aragonite dissolution is negligible at the seafloor but intensifies *ca* 5 m below, even though bulk porewaters are supersaturated for aragonite. This apparent contradiction likely results from dissolution in undersaturated microenvironments. Aragonite dissolution below 5 to 6 m is on average more intense in interglacial compared to glacial intervals. The presence of disseminated framboidal pyrite and porewater results indicate that minor sulphate reduction is active at IODP Site U1460. Sulphate reduction is probably limited by the low organic matter content (*ca* 0.2%). It is well-known from the literature that incipient sulphate reduction can lead to a drop in pH and consequently to carbonate dissolution. It is therefore assumed that the slightly higher concentration of organic matter in the interglacial intervals allowed increased aragonite dissolution during sulphate reduction compared to glacial beds. Low amounts of dolomite cement (<15%) start to form at the same depth (5 to 6 m) as aragonite dissolution intensifies. Dolomite formation and aragonite dissolution also show covariance on a metre-scale below 5 to 6 m, indicating that a low carbonate saturation state might enhance dolomite formation. This mechanism provides an indirect link between dolomite formation, aragonite dissolution and orbital cycles. The outcome of this study, therefore, contributes to a better understanding of differential diagenesis in marine carbonates.

**Keywords** Australia, celestite, differential diagenesis, IODP Expedition 356, IODP Site U1460, Limacina Dissolution Index, Quaternary.

## INTRODUCTION

Aragonite and high-Mg calcite (HMC) are abundant in modern, neritic temperate-water carbonates (James *et al.*, 2005) but are lacking in otherwise similar fossil examples (Wright & Cherns, 2004). Aragonite dissolution in the marine realm can take place in relatively shallow water above the lysocline (Alexandersson, 1978; Smith & Nelson, 2003; James *et al.*, 2005; Dix & Nelson, 2006). For example, the aragonite content on the southern shelf of Australia is reduced from 40 to 90% in Holocene carbonates to 5% in relict carbonate grains, indicating significant aragonite dissolution during the past 20 kyr (Rivers *et al.*, 2008). The original composition of temperate-water carbonates is therefore rapidly modified during early marine diagenesis. Near seafloor carbonate cementation on the other hand is commonly restricted to the formation of intraclasts and sporadic hardgrounds (James & Bone, 1989; James *et al.*, 1999). Overall, cementation of temperate carbonates is relatively slow compared with their tropical counterparts, and micritic envelopes are lacking (James & Bone, 1989). Dissolution of aragonite grains before lithification therefore often leaves no visible imprint, such as mouldic porosity, in the sediment (Brachert & Dullo, 2000). This compromises the ability to derive palaeoenvironmental information from the rock record (Brachert & Dullo, 2000; Wright & Cherns, 2004), since fossil assemblages and even accumulation rates could be altered by this mineral-selective diagenetic loss.

James *et al.* (2005) proposed that aragonite dissolution in temperate carbonates is controlled by the oxic to anoxic degradation of organic matter in the very shallow subsurface, a previously demonstrated important process for aragonite dissolution in tropical carbonates (Walter & Burton, 1990; Ku *et al.*, 1999; Burdige *et al.*, 2010; Drupp *et al.*, 2016). However, it was repeatedly shown that aragonite can be preserved in temperate-water carbonates in outer shelf and slope environments to tens and even hundreds of metres burial depth (Saxena & Betzler, 2003; Deik *et al.*, 2019).

Aragonite undersaturation and dissolution has also been proposed by Rivers *et al.* (2012) as a

prerequisite for the growth of dolomite crystals from saline porewaters in temperate-water carbonates in the Great Australian Bight. At the ODP sites studied by Rivers *et al.* (2012) the dolomite content is on average relatively low (<10%) but variable. Dolomite is also present in the shallow subsurface of many tropical carbonate platforms in small quantities, such as the Bahamas (Swart & Guzikowski, 1988; Dix & Mullins, 1992; Eberli *et al.*, 1997; Swart & Melim, 2000; Murray *et al.*, 2021), the Great Barrier Reef and the Queensland Plateau (Swart, 1993; Dix, 1997). Because of its ubiquity, it is sometimes referred to as 'background dolomite' (Swart & Melim, 2000). It is generally assumed that this dolomite forms in relatively closed diagenetic systems under the influence of marine pore fluids (Murray *et al.*, 2021), with dissolution of HMC and diffusion from seawater being the main sources of  $Mg^{2+}$  (Swart & Guzikowski, 1988; Dix & Mullins, 1992; Swart, 1993; Reuning *et al.*, 2002).

Aragonite and HMC dissolution in marine porewaters therefore seems to be a common, important process in the near seafloor, shallow burial (tens of metres) environment. However, several aspects of this process are insufficiently researched so far: At which burial depth does aragonite dissolution become important in oligotrophic settings that are typically low in organic matter? Does aragonite dissolution increase linearly with depth or does the aragonite dissolution vary periodically with other sedimentary parameters? Is there a relationship between organic matter content and the extent of aragonite dissolution, and does dolomite form preferentially in sediment sections that show more intense aragonite dissolution?

To address these questions, the upper 25 m of core depth at IODP Site U1460 (Gallagher *et al.*, 2017) from the outer Carnarvon Ramp were analyzed. The core contains a nearly complete Middle Pleistocene to Holocene succession of subtropical to cool-water carbonates, covering the glacial to interglacial cycles of Marine Isotope Stages (MIS) 1 to 11 (*ca* 424 kyr). The extent of aragonite dissolution within the sediment was analyzed using the so called Limacina Dissolution Index (LDX), which indicates the

shell preservation in the aragonitic, pelagic gastropod *Heliconoides* (previously *Limacina*) *inflatus* (Gerhardt & Henrich, 2001). The diagenetic processes responsible for dissolution were interpreted from porewater data. Scanning electron microscopy in combination with energy-dispersive X-ray (EDX) data was used to identify dissolution in other sediment grains and cement phases. The concentrations of total organic carbon and the organic biomarker alkenone were measured to evaluate the abundance of reactive organic matter. These methods in combination allow us to link aragonite dissolution, organic matter degradation and carbonate cementation just metres below the seafloor in these temperate carbonates.

### Oceanographic and geological setting

The environment of the western continental margin of Australia in the eastern Indian Ocean is transitional between warm-temperate [*sensu* James & Lukasik (2010), 15–20°C] and tropical carbonate settings. The average sea surface temperature in the vicinity of IODP Site U1460 is 22.5°C with minimum temperatures (20.5°C) in September–October and maximum values of 24.5°C in April (Boyer *et al.*, 2018). Tropical storms in the region are episodic and infrequent, with one or two tropical cyclones affecting the region in one decade (Porter-Smith *et al.*, 2004). In contrast, the significant wave height from wind and swell generated waves in the study area exceeds 3.5 m for 30 to 50% of the time (McMillan, 1982). The seafloor above *ca* 50 to 60 m is therefore subject to constant reworking and abrasion by waves, while the swell wave base is close to 100 m, leading to a lack of mud deposition above this depth (James *et al.*, 1999). Tidal currents are not important for sediment mobilization, with a mean spring tidal current speed of less than 0.2 m s<sup>-1</sup> and spring tidal ranges between 0.5 m and 1.1 m (Porter-Smith *et al.*, 2004).

The IODP Site U1460 is situated below the Leeuwin Current, a southward flowing, warm and oligotrophic eastern boundary current. The Leeuwin Current suppresses wind-driven upwelling and pelagic productivity along the western Australian margin (Godfrey & Ridgway, 1985). Planktonic foraminifera assemblages indicate that the Leeuwin current caused generally oligotrophic conditions offshore north-western Australia over the last *ca* 500 kyr, with possible signs of upwelling restricted to the interglacials MIS 1 and 11 (Spooner *et al.*, 2011). However,

organic matter fluxes at IODP Site U1460 indicate that from around 900 ka to at least *ca* 600 ka productivity was increased during glacials due to the weakening of the warm oligotrophic Leeuwin current (Auer *et al.*, 2021).

The western Australian shelf comprises the Rottnest Shelf in the south (south of 28°S) and the Carnarvon Ramp (Fig. 1A and B) in the north (22 to 28°S). The Houtman Abrolhos Reef complex that is situated at the transition between these two areas (28 to 29.5°S) forms the southernmost major tropical reef in the Indian Ocean (Fig. 1).

The modern sediments on the western Australian shelf are characterized by a distinct cool-water composition (Nelson, 1988), but with subtropical attributes. The skeletal assemblage on the euphotic inner shelf is dominated by coralline algae, bryozoans, molluscs (scaphopods, bivalves and gastropods) and foraminifera, but lacks green algae. The main difference from typical cool-water deposits is the presence of zooxanthellate corals and large, symbiont-bearing foraminifera (James *et al.*, 1999; Collins *et al.*, 2014).

The Carnarvon Ramp comprises the Ningaloo Reef and hypersaline Shark Bay on the inner ramp (Fig. 1A and B). The mid-ramp (*ca* 20 to 100 m) is euphotic, with relatively little calcareous benthos and low numbers of bryozoans, coralline algae and larger foraminifera, but is dominated by relict or stranded foraminiferal-dominated sand. The outer ramp (*ca* 100 to 200 m) is pelagic in character, covered by planktic foraminiferal sand or spiculitic mud. The outflow of highly saline waters from Shark Bay leads to periodic downwelling of relatively warm and saline waters across the ramp (James *et al.*, 1999; Collins *et al.*, 2014). Between 27°N and 28°N the Carnarvon Ramp transitions into the Rottnest Shelf (Fig. 1A and B). The Rottnest Shelf is flat-topped, with a wave-swept, 30 to 70 m deep inner-shelf plain characterized by rhodolith pavements, bryozoans, sponges and abraded sediments (Fig. 1C). An incipient rim (base at *ca* 100 m) formed by a linear ridge system covered by rhodolite gravel separates the inner shelf from the subphotic outer shelf (*ca* 120 to 200 m) that is dominated by bryozoans, benthic foraminifera and molluscs (Fig. 1). This ridge system likely represents a stranded coastal dune system that formed when sea-level was considerably lower than today during MIS3/4 (Fig. 2; Brooke *et al.*, 2014). The upper slope (>150 to 200 m) contains fine sand and silt of

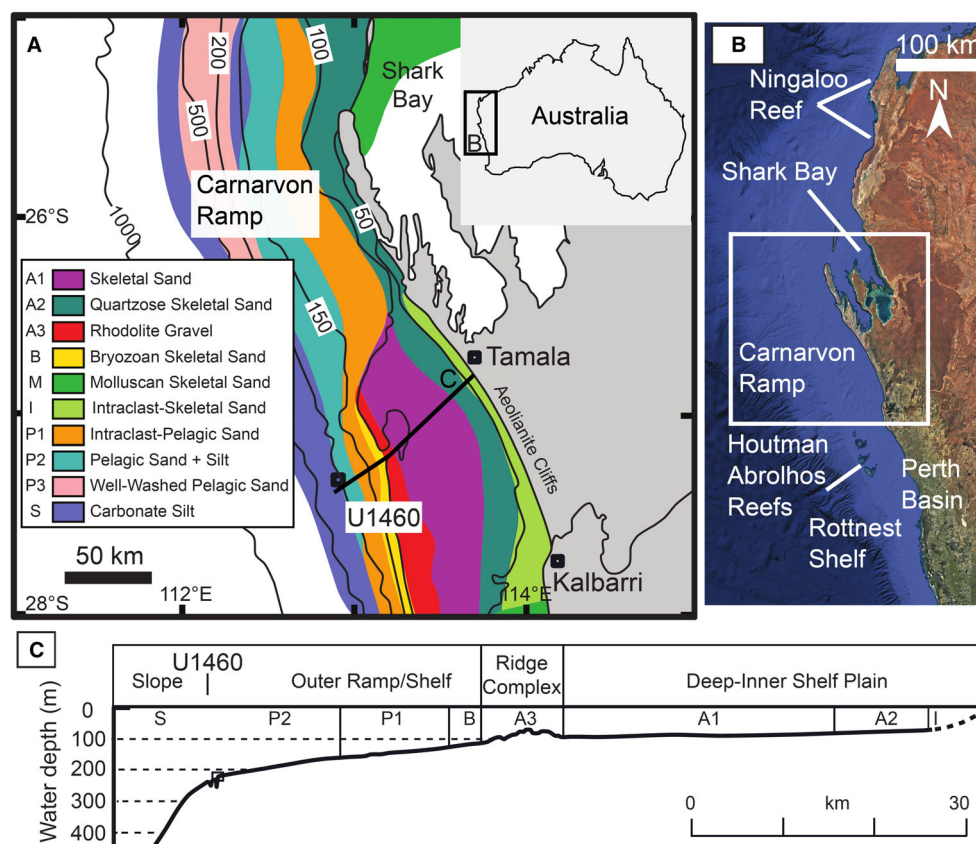


**Fig. 1.** (A) Location map of IODP Site U1460 and sedimentary facies on the modern seafloor of the Carnarvon Ramp/northern Rottneest Shelf, Australia. Bathymetric contours are in metres (modified after James *et al.*, 1999). Black line marks position of profile shown in (C). (B) Satellite map of western Australia. The white box outlines the study area shown in (A) Satellite data: Google Earth, Landsat/Copernicus. (C) Cross-section with distribution of modern facies and location of IODP Site U1460 (modified after James *et al.*, 1999).

bryozoan fragments, sponge spicules and planktic foraminifera (James *et al.*, 1999). This facies extends south to *ca* 34°S on the shelf offshore Cape Leeuwin (Collins, 1988).

On the modern seafloor, syngedimentary cementation is present within intracasts and hardgrounds. Skeletal and lithic intracasts are most abundant in 20 to 200 m water depth on the middle to outer part of the Carnarvon Ramp (James *et al.*, 1999). Cement in intracasts typically consists of micritic, micropeloidal, finely sparitic or sometimes fibrous Mg-calcite (6 to 16 mol.% MgCO<sub>3</sub>). Very similar cements are present in hardgrounds, which occur sporadically in all water depths from the inner shelf to the uppermost slope. Acicular aragonitic cements occur in channels between the Houtman Abrolhos reef platforms on the inner shelf.

During late to Middle Pleistocene glacial intervals, sea surface temperatures were 3 to 5°C

cooler compared to today (Petrick *et al.*, 2019a). This would have terminated reef growth in the region, and carbonate deposition would have been similar to the modern cool-water system on the southern margin of Australia (James *et al.*, 1999). Deik *et al.* (2021) described late to Middle Pleistocene sedimentary cycles at IODP Site U1460 drilled at the uppermost slope of the South-west Shelf of Australia (Fig. 2). They showed a strong control of glacial to interglacial, high amplitude (up to 120 to 130 m; Fig. 2) sea-level changes on the sediment record. In marine isotope stages associated with glacial lowstands, the sediment is characterized by increased HMC and aragonite contents (Fig. 2). The sediment is coarser-grained and neritic components such as bryozoan fragments are more abundant. The intervals have low siliciclastic content, with quartz (4%) as the only significant non-carbonate phase. In contrast, intervals deposited



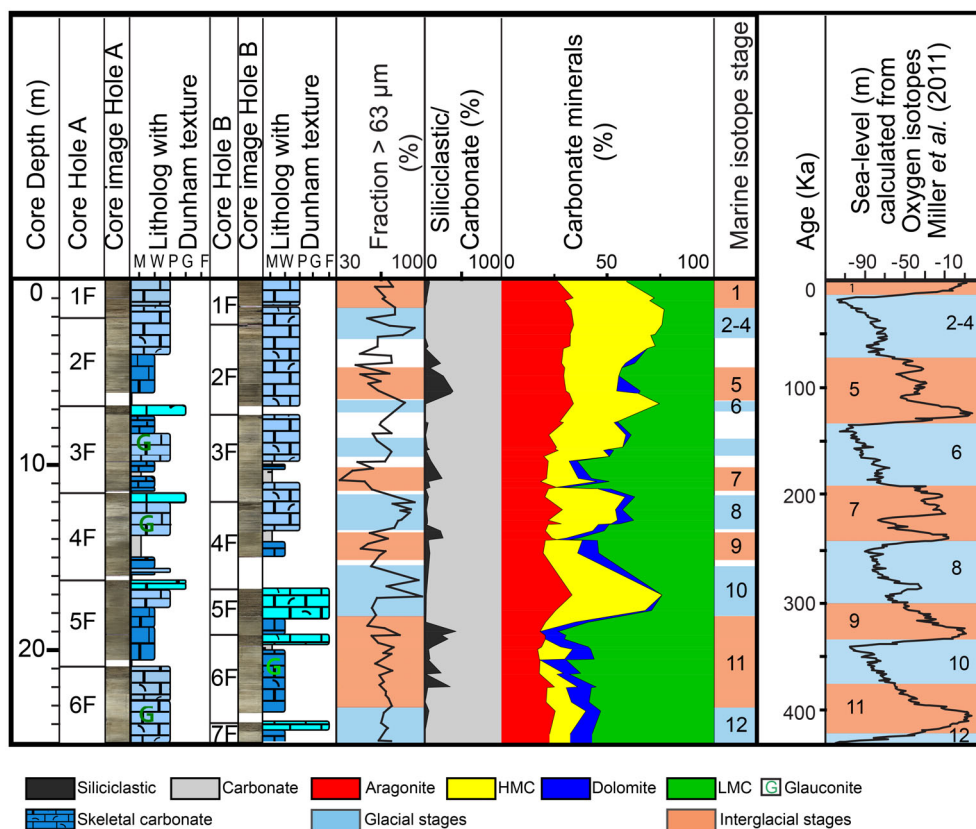


**Fig. 2.** Lithostratigraphic summary for IODP Holes U1460A and U1460B (modified after Deik *et al.*, 2021). Intervals that were attributed by Deik *et al.* (2021) to glacial or interglacial intervals are indicated in colour. Intervals indicated in white could not be attributed unequivocally to either glacial or interglacial periods. The time axis applies only for the sea-level curve. Mineralogy and grain-size fraction are expressed as weight %.

during interglacial sea-level highstands contain more low-Mg calcite (LMC), are finer-grained and show higher concentrations of pelagic material, such as planktic foraminifera. Dolomite is also enriched in interglacial highstand deposits. The siliciclastic content in interglacial intervals is higher (Fig. 2), and plagioclase feldspar is more abundant than quartz.

## MATERIAL AND METHODS

The IODP Site U1460 (27°22.4867'S and 112°55.4265'E; Fig. 1) was drilled in a water depth of *ca* 214 m on the uppermost slope of the South-west Shelf of Australia. Cores were recovered from two boreholes (A and B) at this site (Fig. 2) and drilled with the long hydraulic piston core (HLAPC) system. The sediment recovery in both holes was generally excellent (97 to 98%), with minor gaps between cores

resulting from the HLAPC system (Fig. 2). The cores U1460B-1F to 7F from 0 to 25 m represent a time interval from 0 to 432 ka (Fig. 2; Deik *et al.*, 2021). All depth information is given as core depth below sea floor-A (CSF-A), following IODP conventions (IODP, 2011). The linear sedimentation rate for the entire interval is 5.8 cm kyr<sup>-1</sup>.

On board the *R/V Joides Resolution* interstitial water samples were obtained by squeezing 5 cm long whole-round sections cut from cores (Gallagher *et al.*, 2017). One sample per core was collected and analyzed on board the ship (Gallagher *et al.*, 2017), resulting in sampling increments of *ca* 10 m. Five samples were collected over the uppermost 45 m, with three samples within the target interval of this study. This relatively low-resolution dataset is not sufficient to resolve the metre-scale changes between glacial and interglacial deposits but helps to recognize first order depth related trends in

porewater geochemistry. For this study, the excess or deficit of the diagenetic-active ions  $\text{Ca}^{2+}$ ,  $\text{Mg}^{2+}$ ,  $\text{SO}_4^{2-}$  and  $\text{Sr}^{2+}$  were calculated relative to the conservative element  $\text{Cl}^-$ : Excess (x) = measured (x) – seawater (x) \*  $\text{Cl}^-$  (porewater)/ $\text{Cl}^-$  (seawater).

The thermodynamic modelling package PHR EEQC 3.0 (Parkhurst & Appelo, 2013) was used to calculate the saturation state of aragonite, calcite, dolomite and celestite, using the Pitzer database (Plummer *et al.*, 1988) which is suitable for geochemical calculations in brines to high concentrations. PHREEQC does not consider the influence of total pressure over solubility equilibria of solid phases as well as of aqueous species distribution, but the effect of varying total pressure is minor for carbonates during shallow burial (Arning *et al.*, 2011). Calculations are performed at a fixed total pressure of 1 atm. The temperatures for the calculations are derived from Gallagher *et al.* (2017). Porewater geochemistry is from Gallagher *et al.* (2017) and presented in the results section.

A total of 38 samples were selected to determine the Limacina Dissolution Index (LDX). The LDX, is conventionally used to assess the depths of the aragonite lysocline as a function of oceanic water masses (Gerhardt & Henrich, 2001). However, aragonite dissolution by bottom-waters is highly unlikely at IODP Site U1460, which is situated far above the regional aragonite lysocline (Sabine *et al.*, 2002) and likely was never in significantly deeper water throughout the studied time interval (Haller *et al.*, 2018). The LDX at IODP Site U1460 can therefore be used to assess post-depositional dissolution within the sediment. The LDX methodology involves the qualitative analysis of the shell surface of the pteropod species *Heliconoides inflatus* (synonym: *Limacina inflata*) on a scale from 0 to 5; 0 being a shell that is transparent and lustrous, with a perfect outer aragonite layer, and 5 being a shell that is opaque-white, showing extensive corrosion of the outer aragonite layer (Gerhardt & Henrich, 2001). In addition to the LDX scale from 0 to 5, a scale level of 6 for internal casts (steinkern) with or without only remnants of the original shell preserved was introduced for this study. Additionally, the relative abundance of internal casts of pteropods in the sediment is qualified as absent, low or high (more internal casts compared to number of preserved shells). For each sample, a minimum of ten *H. inflatus* tests from the 125 to 500  $\mu\text{m}$  fraction were

analyzed with a binocular microscope to calculate the mean LDX values. The number of available shells decreased with depth, but more than 30 tests were usually available above 6 m. The method has the advantage that aragonite dissolution can be assessed independently from depositional processes. The total aragonite content, in contrast, is also influenced by variable aragonite input related to sea-level variations (Deik *et al.*, 2021).

Scanning electron microscopy (SEM; Zeiss Supra 55, Carl Zeiss AG, Oberkochen, Germany) was used to analyze the surface of pteropod shells and the bulk sediment. The mineralogy of grains was confirmed by elemental analysis (Sr, S, Fe and Mg) with an energy-dispersive X-ray spectrometer (EDX; Xmax 150, Oxford Instruments, Abingdon, UK). All samples were carbon coated prior to analysis.

Total alkenone abundance throughout the 25 m study interval was measured as a proxy for marine primary productivity. Alkenones are only produced by very specific groups of haptophyte algae, including the widespread coccolithophore *Emiliania huxleyi* and related species (Volkman *et al.*, 1998). These algae are key components of primary productivity (Petrick *et al.*, 2015, 2018) in both open ocean and coastal environments (Salacup *et al.*, 2019). At IODP Site U1460, Auer *et al.* (2021) demonstrated that total alkenone abundance is related to changes in total organic carbon and primary productivity during the Middle Pleistocene.

Alkenone concentrations were measured at the Max Plank Institute of Chemistry in Mainz, Germany. Alkenones were extracted from 60 sediment samples between a depth of 0.01 m and 24.45 m, with a mean sampling resolution of 0.41 m. For analyses, 3 to 5 g of sediment were freeze-dried, gently disaggregated and extracted using a Dionex ASE350 accelerated solvent extraction (ASE) system (Thermo Fisher Scientific Inc., Waltham, MA, USA) using the methods described in Auderset *et al.* (2020). Non-polar (alkenone) fractions were separated using simultaneous extraction and silica separation within the ASE cells and subsequently dried using a Rocket Synergy evaporator (Thermo Fisher Scientific Inc.). Alkenone concentration was determined via an Agilent 7890 B gas chromatography system (Agilent Technologies, Santa Clara, CA, USA) using hexatriacontane and 2-nonadecanone as internal standards, which were added to the sediment before extraction. Throughout the process both blanks and

laboratory standards were used to monitor the recovery of the sample and the width of the peaks to assure high quality data. For more details on the method see Auderset *et al.* (2020). The original weight of the sample was used to normalize the alkenone data. At IODP Site U1460 the alkenone concentrations were well above the detection limit and present throughout the upper 25 m.

The total organic carbon (TOC) content was determined on 12 samples, covering all MIS and nearly the complete range of alkenone concentrations. Aliquots (*ca* 0.1 g) of the freeze-dried and ground samples that were also used for alkenone analyses, were fully decalcified using stepwise addition of 2N HCl. After decalcification, samples were washed with distilled water to remove excess HCl, and dried and measured using a LECO CS300 carbon and sulphur analyzer (LECO Cooperation, St Joseph, MI, USA) at the University of Graz. All measurements were performed in triplicate to evaluate analytical precision as well as sample inhomogeneities. All statistical methods such as the analysis of variance or correlation were carried out using PAST Version 4.0 (Hammer *et al.*, 2001).

## RESULTS

Differences in bulk mineralogy and grain-size between glacial and interglacial intervals can be calculated based on the data presented in Deik *et al.* (2021). The >63 µm fraction (sand and gravel) contributes between 32% and 99% to the sediment with an average of 68%. Glacial intervals have a significantly ( $P < 0.05$ ) higher average content of sand and gravel (77%) compared to interglacial intervals (63%).

The mineralogy is generally dominated by carbonate (91%), with 86% in interglacial and 98% in glacial intervals. This difference is due to an increased contribution of siliciclastic minerals in the interglacial intervals (Fig. 2). Celestite occurs only sporadically ( $n = 4$ ) but never in glacial intervals (Fig. 3). Its average contribution is <1%.

In average, the carbonate component of the studied interval consists of LMC (48%), aragonite (25%), HMC (22%) and dolomite (5%). There is a general trend to increasing LMC and dolomite contents with depth. On the other hand, aragonite and HMC show a tendency to decrease with depth. This is especially apparent for a comparison between the average aragonite and HMC values in the interglacial intervals of the upper *ca*

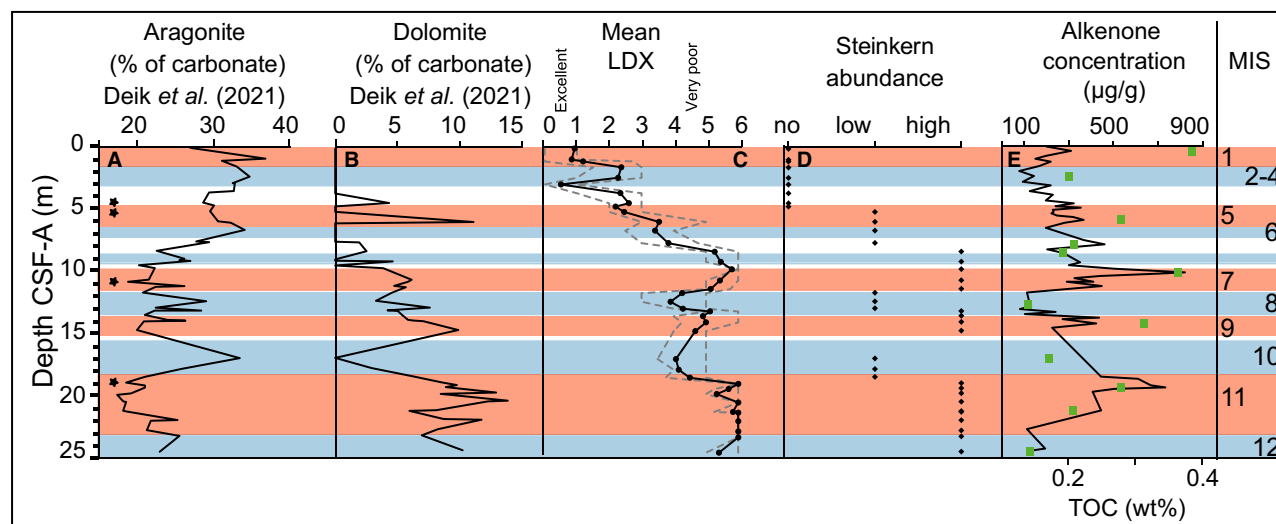


**Fig. 3.** Mineralogy, aragonite dissolution (LDX and steinkern abundance), total organic carbon (TOC) and alkenone concentrations. (A) Aragonite content of carbonate. The occurrence of celestite is indicated by asterisks (\*). (B) Dolomite content of carbonate [data for (A) and (B) are from Deik *et al.* (2021)]. (C) The mean LDX data (solid line) shows a shift from excellent and very good preservation (LDX 0 to 2) to poor and very poor preservation (LDX 3 to 5) between 5 m and 6 m. The lower quartile and the upper quartile of the LDX data are indicated by dashed grey lines. (D) Internal casts (steinkern), start to occur between 5 m and 6 m. (E) Alkenone concentration and TOC (green rectangles) in the sediment. Glacial (blue) and interglacial (pink) marine isotope stages (MIS) are indicated in colour. Intervals in white were not unequivocally associated to glacial or interglacial periods (see Fig. 2).



6 m (MIS 1 and 5) with the interglacial intervals below this depth (MIS 7, 9 and 11). Aragonite values are reduced by about one-third from 31% to 21%, while HMC values are reduced by about two-thirds from 31% to 10% between the two intervals. Aragonite shows a significant ( $P < 0.05$ ) and strong positive correlation with HMC ( $r^2 = 0.58$ ) and a significant ( $P < 0.05$ ), moderate negative correlation ( $r^2 = 0.32$ ) to LMC. Dolomite shows a significant ( $P < 0.05$ ) and strong negative correlation with aragonite ( $r^2 = 0.52$ ) and HMC ( $r^2 = 0.57$ ), if only carbonate phases are considered (see Appendix S1). Generally, interglacial intervals are characterized by a higher LMC content (55% of carbonate) compared to glacial intervals (39%). Aragonite and HMC contents are higher in glacial intervals (28% and 30%) relative to interglacial intervals (23% and 15%). The Mg-content of calcite cements as measured by EDX ranges between 4 mol. % and 12 mol. %. Measurable quantities of dolomite are only observed below 4 m (Fig. 3) and below this depth is more abundant in interglacial (7%) than in glacial intervals (4%). This is confirmed by SEM observations indicating that dolomite cements (Fig. 4A and B) preferentially, but not exclusively, occur in interglacial intervals. All of these average values in mineralogy are significantly different ( $P < 0.05$ ) between glacial and interglacial intervals.

The LDX record indicates excellent preservation (0 to 1) of aragonitic pteropod shells in the uppermost metre of the core (Figs 3, 5A and 5B). This is in accordance with the position of IODP Site U1460 far above the regional lysocline (Sabine *et al.*, 2002). From 1 m to ca 5 m the LDX indicates excellent to moderate (0 to 3) preservation (Fig. 3). The first occurrence of very poorly preserved, perforated shells (LDX 4 to 5; Fig. 5C and D) in a generally moderately preserved shell assemblage at ca 2 m indicates that aragonite dissolution starts during very shallow burial. Excellently and very poorly preserved shells often are found in the same sample, which results in relatively large quartile ranges in some of the samples (Fig. 3). Below 6 m the transparent shells (LDX 0; Fig. 5A and B) are absent and the mean LDX indicates poor (LDX 3 to 4; Fig. 5C) to very poor (LDX >4; Fig. 5D) preservation. Internal casts of pteropod shells, many with preserved remnants of the original shell, are only present at depth greater than 5 m (Figs 3, 5E and 5F). The abundance of internal casts is generally higher during interglacials compared to glacials. Below 6 m, the preservation of pteropod shells is generally very poor but somewhat greater in glacial (LDX: 5) compared to interglacial (LDX: 6;  $P < 0.05$ ) intervals (Fig. 3). Below 10 m, the number of well-preserved pteropod shells in

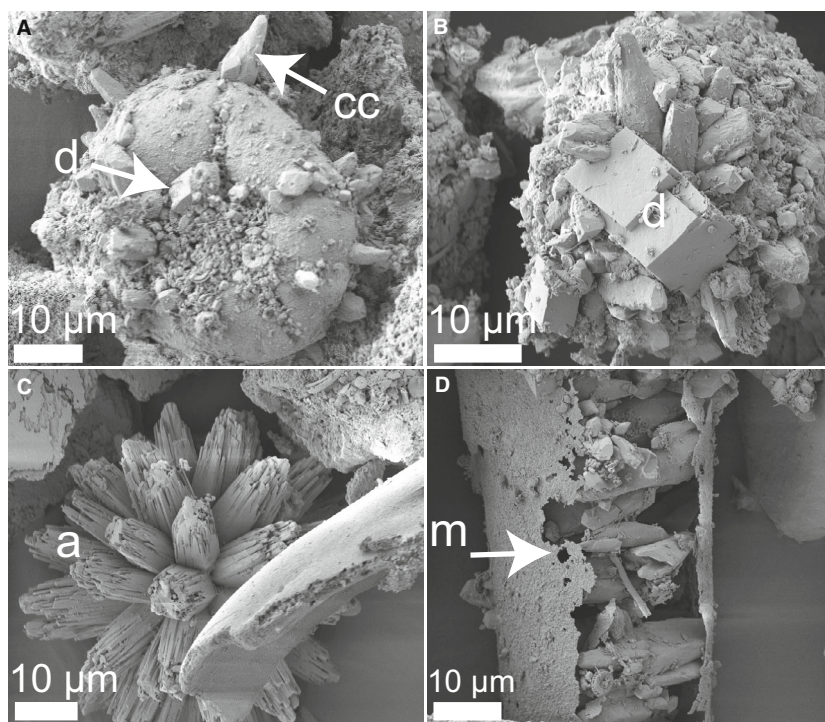


**Fig. 4.** Scanning electron microscope (SEM) pictures of aragonitic components and diagenetic phases. (A) Dolomite cement (d) and calcite cement (cc) (356-U1460B-5F-2W 79/83). (B) A dolomite cement crystal partially grown around a bioclastic calcite grain (356-U1460B-5F-2W 79/83). (C) Ascidian (a) spicule (356-U1460B-1F-1W-115/119). (D) Partly dissolved aragonitic bivalve shell (m, arrow) (356-U1460B-5F-2W 79/83).



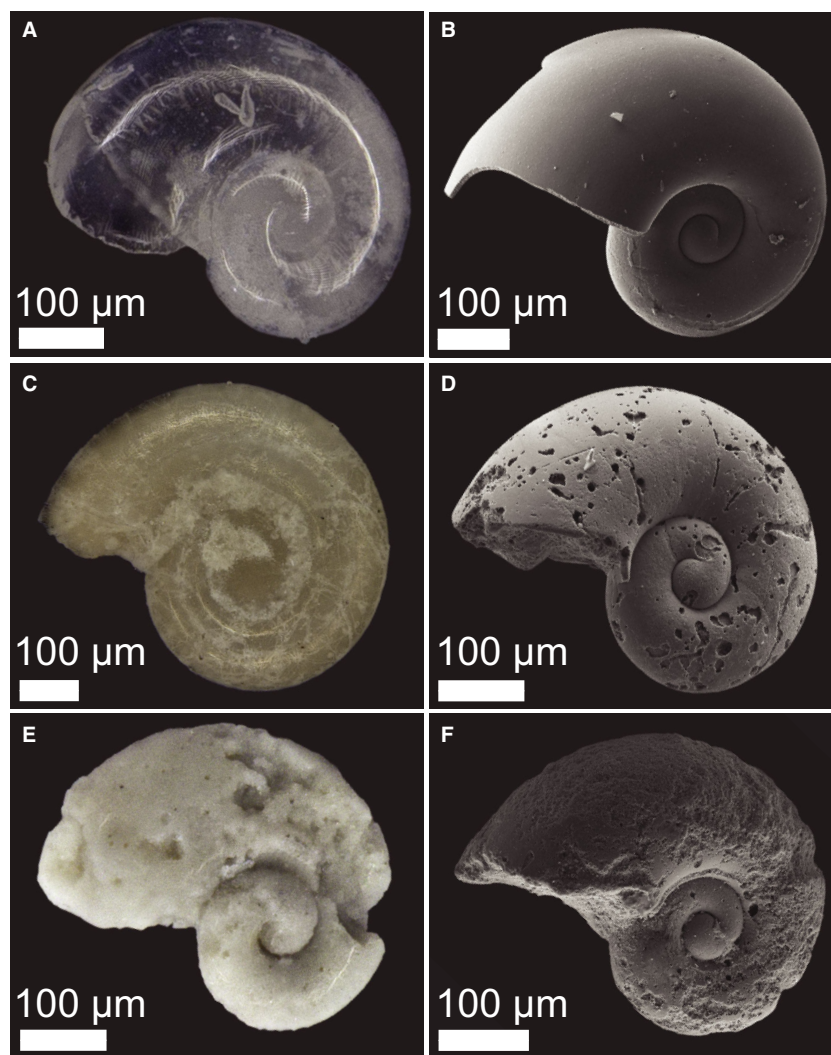


**Fig. 5.** *Heliconoides inflatus* (synonym: *Limacina inflata*) shell preservation as a proxy for aragonite dissolution according to the *Limacina* dissolution index (LDX). (A) to (F) show different stages of shell preservation typical for LDX stages with pictures from binocular and scanning electron microscopy on the left and right side, respectively. (A) and (B) LDX stage 0: transparent shells indicate best preservation (356-U1460B-1F-1W 12/16). (C) and (D) Milky (LDX stage 4, left) and perforated shells (LDX stage 5), indicate strong dissolution (356-U1460B-1F-2W 12/13). (E) and (F) Nearly complete dissolution of shells (LDX stage 6) produces internal casts (steinkern) (356-U1460B-3F-4W 40/44).

interglacial intervals decreases. The presence of internal casts in the same intervals indicates that pteropods were present but scarcely preserved. Below a depth of 18 m the shells generally show very poor preservation (Fig. 3). The internal casts are partially cemented by dolomite and subordinate intermediate-Mg calcite (IMC, a calcite with 4 to 12 mol.%  $\text{MgCO}_3$ ) cements. Dissolution of aragonitic skeletal grains, such as tunicate spicules and bivalve shells (Fig. 4C and D), can be clearly detected below *ca* 5 m using SEM.

Total organic carbon values are generally low and vary between 0.14% and 0.39%, with a mean of 0.24% ( $n = 12$ ; Fig. 3). The average TOC of interglacial intervals (0.3%) is significantly ( $P < 0.05$ ) higher compared to glacial intervals (0.17%) and each interglacial shows a peak in TOC values relative to adjacent glacial intervals.

The alkenone concentration varies between 80 and  $820 \mu\text{g g}^{-1}$ , with an average of  $300 \mu\text{g g}^{-1}$  ( $n = 60$ ; Fig. 3), with peaks in alkenone concentrations in interglacials 7 and 11. Average alkenone concentrations of all interglacial intervals ( $375 \mu\text{g g}^{-1}$ ) are significantly ( $P < 0.05$ ) higher compared with all glacial intervals ( $158 \mu\text{g g}^{-1}$ ). Average alkenone concentrations of interglacials are typically significantly ( $P < 0.05$ ) higher compared to their adjacent glacials, except for MIS 5 and MIS 6 which show nearly identical average values. Total organic carbon values show a strong ( $r^2 = 0.4$ ), and significant ( $P < 0.05$ ), positive correlation with the alkenone concentrations.

Concentrations of  $\text{Cl}^-$ ,  $\text{Sr}^{2+}$ ,  $\text{Mg}^{2+}$ ,  $\text{Ca}^{2+}$ , sulphate and alkalinity in the porewater at IODP Site U1460 (Gallagher *et al.*, 2017; Fig. 6) exceed average and regional seawater concentrations (Dickson & Goyet, 1994; De Deckker, 2004;

Olsen *et al.*, 2016, 2019). The systematic increase in salinity to 41 psu at *ca* 43 m is paralleled by  $\text{Cl}^-$  (Fig. 6A). Alkalinity,  $\text{Ca}^{2+}$  and  $\text{Mg}^{2+}$ -ion concentrations show a similar general increase with depth, albeit less linear (Fig. 6B and C). The pH drops rapidly to values around 7.7 in the sample at *ca* 10 m and all other samples below.  $\text{Sr}^{2+}$  concentrations increase rapidly with depth to values between 500  $\mu\text{M}$  and 600  $\mu\text{M}$  at a depth of *ca* 19 m and stays nearly constant below this depth (Fig. 6D). The sulphate concentrations in the porewater are higher compared to normal seawater and are relatively constant with depth (Fig. 6D).

Diagenetic processes in the sediments can be identified by an excess or deficit of diagenetically active ions relative to conservative ones, such as  $\text{Cl}^-$ . Normalizing cations and anions against  $\text{Cl}^-$  therefore can help to identify and evaluate water–rock interactions (Fig. 6E).  $\text{Mg}^{2+}$  concentrations show a deficit of more than  $-3$  mM in a sampling depth of *ca* 19 m and in samples below this depth.  $\text{Ca}^{2+}$  concentrations show only a very small deficit at *ca* 10 m but an excess of around 1 to 3 mM for the samples at *ca* 19 m and below. In samples from *ca* 19 m and below the sulphate concentrations show a deficit of more than 1 mM. The sample from about 10 m shows a very low sulphate deficit of less than 1 mM, while the sulphate depletion is negligible at *ca* 1 m below the seafloor. Alkalinity shows an excess of around 1 mM at *ca* 1 m and 10 m, which increases to close to 2 mM in samples at *ca* 19 m and below. The excess of  $\text{Sr}^{2+}$  increases to approximately 500  $\mu\text{M}$  at *ca* 19 m and stays nearly constant in samples below this depth.

Samples at all depths show a supersaturation with respect to aragonite, LMC and dolomite (Fig. 6F). The sample at *ca* 10 m shows the lowest supersaturation for all carbonate phases. Samples below this depth show a minor but constant increase in saturation. The porewater is undersaturated with respect to celestite at *ca* 1 m and approaches equilibrium at around *ca* 10 m. Samples below this depth show a constant oversaturation with respect to celestite.

## DISCUSSION

### Carbonate dissolution

It is well-known that dissolution of aragonite in the shallow subsurface (tens of metres) is an

important process in tropical and temperate carbonates (Swart & Guzikowski, 1988; Dix & Mullins, 1992; Brachert & Dullo, 2000; James *et al.*, 2005; Rivers *et al.*, 2008). The LDX is a very sensitive indicator of aragonite dissolution (Gerhardt & Henrich, 2001). Wall-Palmer *et al.* (2013) postulated that pteropod shells might be affected by aragonite dissolution during their lifetime, or after death in the water column (Oakes & Sessa, 2020) even in aragonite supersaturated waters. The excellent preservation of pteropods to a burial depth of 1 m below the seafloor at IODP Site U1460A confirms that dissolution did not take place during the lifetime of the pteropods, in the water column after death or at the seafloor. At this location, the LDX can therefore be used to track dissolution during shallow burial below the seafloor. The LDX record at IODP Site U1460 (Fig. 3) shows a trend from negligible dissolution (LDX 0 to 2) to strong dissolution (LDX 3 to 5) from 5 to 6 m. At around the same depth, the abundance of internal casts of pteropods increases significantly, confirming that the LDX is recording aragonite dissolution within the sediment.

The LDX record is consistent with porewater measurements showing that normalized  $\text{Sr}^{2+}$  concentrations (Fig. 6E) are close to seawater values at *ca* 1 m but increase to *ca* 300  $\mu\text{M}$  in a depth of *ca* 10 m. Aragonite usually contains much higher Sr contents compared with calcite and dolomite (Milliman *et al.*, 1974). A rapid increase in the  $\text{Sr}^{2+}$ -concentration of porewaters, such as at IODP Site U1460, therefore is best explained by aragonite dissolution.  $\text{Sr}^{2+}$  concentrations in pteropod shells are relatively low (*ca* 1000 ppm), but other aragonite skeletal components that show evidence of dissolution, such as tunicate spicules (Fig. 4C; Deik *et al.*, 2019), contain 8000 to 9000 ppm Sr (Milliman *et al.*, 1974). Porewater samples at *ca* 19 m and below show constant, normalized  $\text{Sr}^{2+}$ -concentrations of *ca* 500  $\mu\text{M}$  (Fig. 6E). A further increase of  $\text{Sr}^{2+}$  concentrations is likely prevented by celestite ( $\text{SrSO}_4$ ) precipitation (Figs. 3), when bulk porewaters become supersaturated with respect to this mineral in depths between *ca* 10 m and 19 m (Fig. 6F). Relatively constant, normalized  $\text{Sr}^{2+}$ -concentrations at *ca* 19 m and below therefore do not indicate the absence of aragonite dissolution, but the incorporation of  $\text{Sr}^{2+}$  from the porewater into celestite. This is a common process in aragonitic, platform derived sediments (Swart & Guzikowski, 1988). The precipitation of celestite at a shallow depth of *ca* 5 m (Fig. 3)

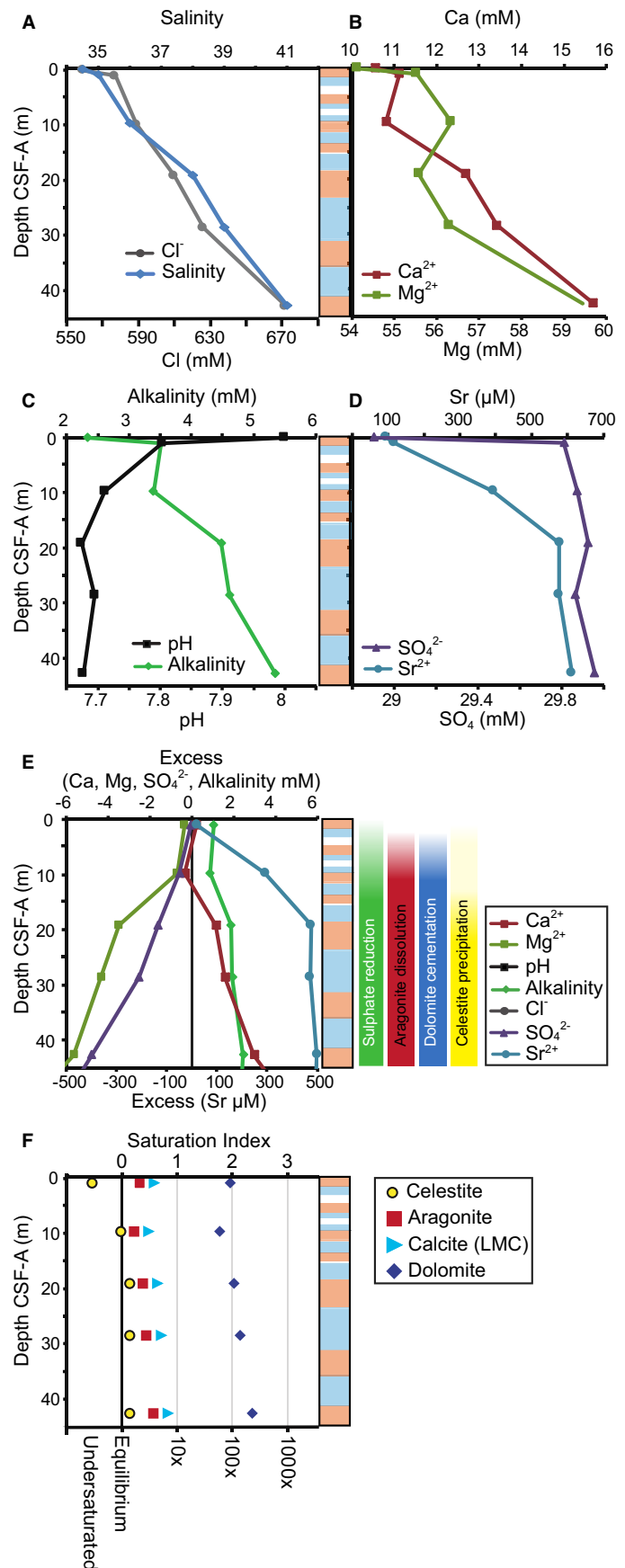


**Fig. 6.** (A) to (D) Porewater profiles at IODP Site U1460 (Gallagher *et al.*, 2017); literature values for seawater composition (Dickson & Goyet, 1994; Deckker, 2004; Olsen *et al.*, 2016, 2019) are plotted at the depth of the seafloor. (E) Excess (positive) and deficit (negative deviation) of non-conservative elements relative to  $\text{Cl}^-$ . The colour bars indicate the depth intervals in which diagenetic processes are interpreted to be active and the resultant diagenetic phases formed. (F) Saturation indices for celestite, aragonite, calcite (LMC) and dolomite calculated from porewater data. Glacial (blue) and interglacial (pink) marine isotope stages (MIS) are indicated in colour.



is favoured by the sulphate-rich porewater at IODP Site U1460 (Fig. 6D).

The presence of common aragonite dissolution is therefore shown by  $\text{Sr}^{2+}$ -porewater data and SEM observations (Fig. 4C and D). Based on LDX (Figs 3 and 5), the aragonite dissolution becomes important at a depth between 5 m and 6 m. However, the saturation state calculations indicate that porewaters are supersaturated with respect to aragonite at all sampled depths (Fig. 6F). This apparent contradiction could either result from higher than expected aragonite solubility or from aragonite undersaturated microenvironments in the sediment.

First, microstructural complexity of carbonate grains can override thermodynamic constraints and lead to selective dissolution (Walter & Morse, 1985). Bednaršek *et al.* (2014) have shown for one pteropod species that shell dissolution occurs even in slightly oversaturated seawater. Pteropods and other biogenic aragonite grains with a high microstructural complexity could therefore show signs of dissolution even in slightly oversaturated porewaters.

Second, the dissolution might be controlled by patchily distributed, aragonite undersaturated microenvironments (Sanders, 2003). Individual pteropod shells with very different preservation states have been observed within one sample, as indicated by the relatively large spread of the quartile values around the mean LDX (for example, at 6 m; Fig. 3). This could indicate that they have been diagenetically altered in microenvironments with different saturation states. Celestite cements, impregnating a bioturbation trace found at 119.65 m (Gallagher *et al.*, 2017), also indicate that microenvironments might be important for dissolution/precipitation reactions at the site. Bulk porewater data were produced from 5 cm long whole-round sections cut from cores, which have a much larger sample volume compared to the samples used for LDX analysis. The measured porewater therefore could be derived from different microenvironments with variable saturation states with respect to aragonite, as indicated by the large spread in LDX data around the mean in many samples (Fig. 3). The microstructural complexity of the biogenic grains and the patchy distribution of undersaturated microenvironments therefore likely enable the dissolution of aragonitic bioclasts, even though the bulk porewater is calculated to be supersaturated with respect to aragonite. This could also explain the general reduction of aragonite content in the bulk mineralogy with depth (Fig. 3).

The fate of HMC is more difficult to evaluate. High-Mg calcite with 4 to 12 mol. % Mg occurs as a subordinate cement phase in pore spaces (Fig. 4A). The solubility of calcite increases with its Mg-content, while biogenic HMC with *ca* 12 mol. % Mg is as soluble as aragonite (Walter & Morse, 1984). Because of their Mg-content which usually are <12 mol. % Mg, most of these cements are less soluble compared to aragonite. Even cements with 12 mol. % Mg are likely more stable than aragonite, since cements are typically less soluble than their biogenic counterparts with equivalent Mg content (Morse & Mackenzie, 1990). The Mg-calcite cements could have formed during burial or prior to burial at the seafloor, since cemented intraclasts and incipient hardgrounds exist at the modern-day seafloor at the mid to outer ramp (James *et al.*, 1999).

The observed aragonite dissolution could imply that at least the HMC with >12 mol. %  $\text{MgCO}_3$  could also have been affected by dissolution. The decrease of HMC content with depth (Fig. 2) could therefore either result from the loss of  $\text{Mg}^{2+}$  from the HMC crystal lattice during recrystallization to more stable LMC (i.e. incongruent dissolution), or by preferential but complete dissolution of the more soluble HMC with high Mg-contents. The first process was invoked in periplatform carbonates off north-eastern Australia by Brachert & Dullo (2000), whereas the second process is consistent with Rivers *et al.* (2008), who observed that HMC grains become partially dissolved instead of being recrystallized to LMC. Both of these processes would reduce the relative abundance of HMC, which could explain the reduction of HMC with depth at IODP Site U1460 (Fig. 2).

It is generally accepted that carbonate dissolution in the shallow burial zone is controlled by processes involving organic matter degradation. This has also been postulated for the slopes and margins of several modern carbonate platforms (Swart & Guzikowski, 1988; Dix & Mullins, 1992; Brachert & Dullo, 2000; James *et al.*, 2005).

The near-seafloor diagenetic processes active at IODP Site U1460 can be constrained using the porewater profiles (Fig. 6). The salinity-increase with depth (Fig. 6A) likely reflects mixing of seawater with saline brines from the underlying Miocene section. Sites U1461 to U1464, all on the North-West Shelf of Australia, show a continuous increase in salinity towards their respective Miocene sections (Gallagher *et al.*, 2017). A

Miocene sabkha sequence containing anhydrite was drilled during IODP Expedition 356 on the North-West Shelf of Australia (Gallagher *et al.*, 2017). The sabkha shows similar characteristics to Holocene sabkhas from the Trucial coast, indicating very arid and hypersaline conditions (Groeneveld *et al.*, 2017; Petrick *et al.*, 2019b). The increased salinity and relatively high sulphate concentration in the porewater therefore likely results from upward diffusion of saline and sulphate-rich brines (Fig. 6A and D).

After normalization against  $\text{Cl}^-$ , it becomes apparent that sulphate does not simply increase with salinity and  $\text{Cl}^-$  but shows a deficit of more than 1 mM in samples at *ca* 19 m and below. The sample at *ca* 10 m is characterized by only a small sulphate deficit of less than 1 mM, while sulphate depletion closer to the seafloor (*ca* 1 m) is negligible (Fig. 6E). Sulphate reduction therefore must begin to influence porewater somewhere between the samples at 1 m and 10 m. Framboidal pyrite, indicating bacterial sulphate reduction, was observed as shallow as *ca* 1 m (Deik *et al.*, 2019). The fact that the porewaters indicate only negligible sulphate reduction at this depth, likely indicates that sulphate reduction is restricted to few microenvironments. Alternatively, it could be explained by re-oxidation of sulphide to sulphate which could maintain near normal sulphate concentrations despite active sulphate reduction (Ku *et al.*, 1999).

Overall, the sulphate concentration increases with depth (Fig. 6D) despite the consumption during sulphate reduction (Fig. 6E). This indicates that the rates of sulphate reduction seem to be low compared to the upward diffusion of sulphate ions. The low sulphate reduction potential could result from the low availability of total organic matter at this site, with overall low alkenone concentrations and TOC ranging only between 0.1% and 0.4% (Fig. 3). These low alkenone and TOC values likely result from the generally oligotrophic conditions at IODP Site U1460 during the last *ca* 0.6 Myr, as indicated by benthic foraminifera assemblages (Haller *et al.*, 2018).

Oxidation of organic matter during sulphate reduction in a closed system is accompanied by an initial drop in pH (Ben-Yaakov, 1973). The sample at *ca* 10 m shows a pH of 7.7, about 0.3 units lower compared to regional seawater concentrations (Olsen *et al.*, 2016, 2019), leading to the lowest calculated aragonite saturation state of all samples (Fig. 6F). These pH values likely are either caused or maintained by the incipient sulphate reduction at this depth (Fig. 6E). The

deduced onset of sulphate reduction in porewaters between the samples at *ca* 1 m and *ca* 10 m, therefore, could decrease the aragonite saturation and would be broadly consistent with the increase in dissolution observed based on a LDX between 5 to 6 m.

Superimposed on this general depth trend, the pteropod shell preservation (LDX and internal casts) shows variability on a metre-scale. Below 6 m, the pteropod shells are better preserved in glacial compared to interglacial intervals (Fig. 3). The porewater sampling is not sufficiently high to help with interpreting these metre-scale alterations in aragonite dissolution. However, aragonite dissolution is stronger in the interglacial intervals that also show increased TOC values of up to 0.4%, while the glacial intervals show less aragonite dissolution and TOC values as low as 0.1%. It is therefore assumed that the higher TOC values observed in interglacial intervals allow sulphate reduction of a few mM sulphate, resulting in a pH decrease (Ben-Yaakov, 1973) and an increase in the number of microenvironments undersaturated with respect to aragonite.

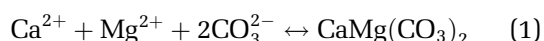
At IODP Site U1460, the higher concentrations of organic matter in the interglacial intervals might be related to their higher fine-fraction content ( $<63 \mu\text{m}$ ; Fig. 2). Fine-grained particles have a high capacity for organic matter adsorption due to their large specific surface area (Hedges & Keil, 1995). Alternatively, the higher alkenone and organic matter concentrations could be associated with upwelling events during interglacial periods along the western Australian margin (Spooner *et al.*, 2011). Such a relationship between carbonate dissolution in the sediment, upwelling and suboxic organic matter remineralization was already demonstrated by Schulte & Bard (2003) for a deep-sea core from the Indian Ocean. They showed that calcite dissolution within the sediment is highly coherent and in phase with orbital controlled palaeoproductivity variations, providing strong evidence for a control of organic matter remineralization on the observed dissolution pattern. A similar cyclic pattern in aragonite dissolution driven by orbital controlled palaeoproductivity variations has been postulated for periplatform sediments from the Maldives (Reuning *et al.*, 2006; Deik *et al.*, 2017).

## Dolomite formation

Dolomite formation at IODP Site U1460, which never exceeds an abundance of 13% in bulk

sediment (Fig. 2), occurs below a depth of *ca* 5 m. Its shallowest occurrence downcore therefore coincides with the onset of aragonite dissolution based on the LDX (Fig. 3). Dolomite abundance generally increases downcore, but also shows metre-scale variability with higher average values in interglacial intervals that on average also show more intense aragonite dissolution (Fig. 3). Rivers *et al.* (2012, 2019, 2021) proposed that a low calcium carbonate saturation in porewaters might be crucial to drive dissolution–precipitation reactions causing dolomite formation. Observations from the current study seem to fit this pattern but show that bulk porewaters do not have to be undersaturated with respect to aragonite for the formation of this type of dolomite (Fig. 6F). Instead, aragonite dissolution and dolomite precipitation are thought to occur in microenvironments undersaturated with respect to aragonite.

Dolomite at IODP Site U1460 was only present as dolomite cement (Fig. 4A and B) and not as replacement product. Precipitation of dolomite cement following Eq. 1 should consume  $\text{Mg}^{2+}$ ,  $\text{Ca}^{2+}$  and alkalinity from the porewater:



Porewater data at *ca* 10 m show a slight deficit of  $\text{Mg}^{2+}$  and  $\text{Ca}^{2+}$ , consistent with the removal by dolomite cementation. The amount of  $\text{Mg}^{2+}$  removal indicated by the porewater data likely is not enough to form the *ca* 5% dolomite at this depth. Two possible sources for  $\text{Mg}^{2+}$  are: (i) diffusion from seawater and the saline porewaters; and (ii) the dissolution of HMC or its stabilization to LMC. Both processes would be in line with the observed clear negative correlation between HMC and dolomite content. At *ca* 19 m and below the  $\text{Mg}^{2+}$  deficit increases, while there is an excess of  $\text{Ca}^{2+}$ . The most likely explanation for the excess of  $\text{Ca}^{2+}$  in porewater at this depth is the observed dissolution of aragonite (Figs 3, 4C, 4D and 5).

Dolomite cement likely formed in porewaters affected by sulphate reduction, as indicated by the porewater samples at *ca* 10 m and below. Dolomite formation could potentially be favoured by the presence of sulphate reducing bacteria. Microbes can play an important role in overcoming the kinetic barriers for low temperature precipitation of dolomite and HMC (Van Lith *et al.*, 2003; Wright & Wacey, 2005; Krause *et al.*, 2012), although the exact mechanisms are not well-understood. Alternatively, or

additionally,  $\text{H}_2\text{S}$  produced during bacterial sulphate reduction could act as a catalyst for the precipitation of dolomite at low temperatures (Zhang *et al.*, 2012).

An obvious effect of sulphate reduction is that it increases the carbonate alkalinity in the porewaters, with a two-fold increase of alkalinity for each mol of sulphate consumed (Ben-Yaakov, 1973). The alkalinity excess is less than expected in porewater samples at *ca* 19 m and below (Fig. 6E), which is best explained by consumption of excess alkalinity by the precipitation of dolomite cement. The increase in alkalinity associated with sulphate reduction is also the main reason for the higher carbonate saturation levels at *ca* 19 m and below compared to shallower porewater samples (Fig. 6F). The precipitation of dolomite likely is facilitated by these higher saturation levels, as long as microenvironments are still undersaturated with respect to more kinetically favourable carbonate phases.

Overall the mechanism for dolomite formation outlined above is similar to the findings from many other modern carbonate platform margins and slopes worldwide, such as the Bahamas (Swart & Guzikowski, 1988; Dix & Mullins, 1992; Swart & Melim, 2000; Murray *et al.*, 2021), the Great Barrier Reef and Queensland Plateau (Swart, 1993; Dix, 1997) and the Great Australian Bight (Rivers *et al.*, 2012). Dolomite is present in the shallow subsurface of these platforms in low amounts of typically not more than 10 to 15%. It is sometimes called ‘background dolomite’ (Swart & Melim, 2000), due to its ubiquity. This dolomite is commonly assumed to form in relatively closed diagenetic systems under the influence of marine pore fluids (Murray *et al.*, 2021), with dissolution of HMC and diffusion from the seawater as the main sources for  $\text{Mg}^{2+}$  (Swart & Guzikowski, 1988; Dix & Mullins, 1992; Swart, 1993; Reuning *et al.*, 2002). The undersaturation with respect to aragonite and its consequent dissolution is often seen as a prerequisite for the formation of dolomite (Rivers *et al.*, 2012). The mechanism of dolomite formation interpreted for IODP Site U1460 therefore seems to be typical for platform margin and slope systems from the temperate and tropical zone that consist of mixed carbonate mineralogy (aragonite, HMC and calcite). The application of the aragonite dissolution proxy LDX in this study shows that metre-scale variations in dolomite abundance coincide with changes in aragonite dissolution intensity.



In summary, the glacial and interglacial sediments in the upper 25 m at IODP Site U1460 show primary differences in texture and mineralogy (Figs 2 and 7). Glacial packstones are on average aragonite-rich compared to interglacial wackestones (Figs 2 and 7). Interglacial deposits in contrast are on average characterized by higher organic carbon (OC) contents (Figs 3 and 7). Aragonite dissolution begins *ca* 5 to 6 m below the seafloor (Fig. 3). Below this depth, aragonite dissolution (as indicated by LDX) is more intense in the, on average, more organic-carbon rich interglacial deposits, likely enhancing the primary difference in mineralogy (Fig. 7). The dissolution of aragonite provides  $\text{Sr}^{2+}$  for the precipitation of celestite ( $\text{SrSO}_4$ ) in interglacial sediments (Figs 6E, 6F and 7). Additionally, HMC is losing  $\text{Mg}^{2+}$  to the porewater that is incorporated during the precipitation of dolomite in interglacial deposits (Figs 6E and 7). In glacial deposits these processes are presumably much less intense due to the lower average concentration of organic carbon.

## Implications

The LDX values at IODP Site U1460 indicate excellent to good preservation of aragonite in

the uppermost 5 m of core covering the last glacial–interglacial cycles (Fig. 3). Synsedimentary aragonite dissolution such as observed in temperate carbonate shelf sediments of the Great Australian Bight (Rivers *et al.*, 2008), therefore seem to be negligible in this outer ramp to upper slope setting. This can likely be explained by the higher sedimentation rate at the outer ramp position of our study site compared to the palimpsest shelf sediments of the Great Australian Bight studied by Rivers *et al.* (2008). Below a depth of 5 m, the trend in LDX to poor preservation is superimposed by a cyclic component, showing better preservation in glacial compared to adjacent interglacial intervals. This is important since increased LDX values during interglacials have been attributed to stronger in-life dissolution of pteropod shells due to increased atmospheric  $\text{CO}_2$  (Wall-Palmer *et al.*, 2013; Sreevidya *et al.*, 2019). However, the correlation of LDX with steinkern abundance shows that LDX at IODP Site U1460 is not a record of in-life dissolution or dissolution within the water column but of variable dissolution within the sediment (Fig. 3). Studies using LDX as indicator of in-life dissolution or bottom water corrosiveness often interpret LDX depth trends as diagenetically controlled, while cyclic changes are often

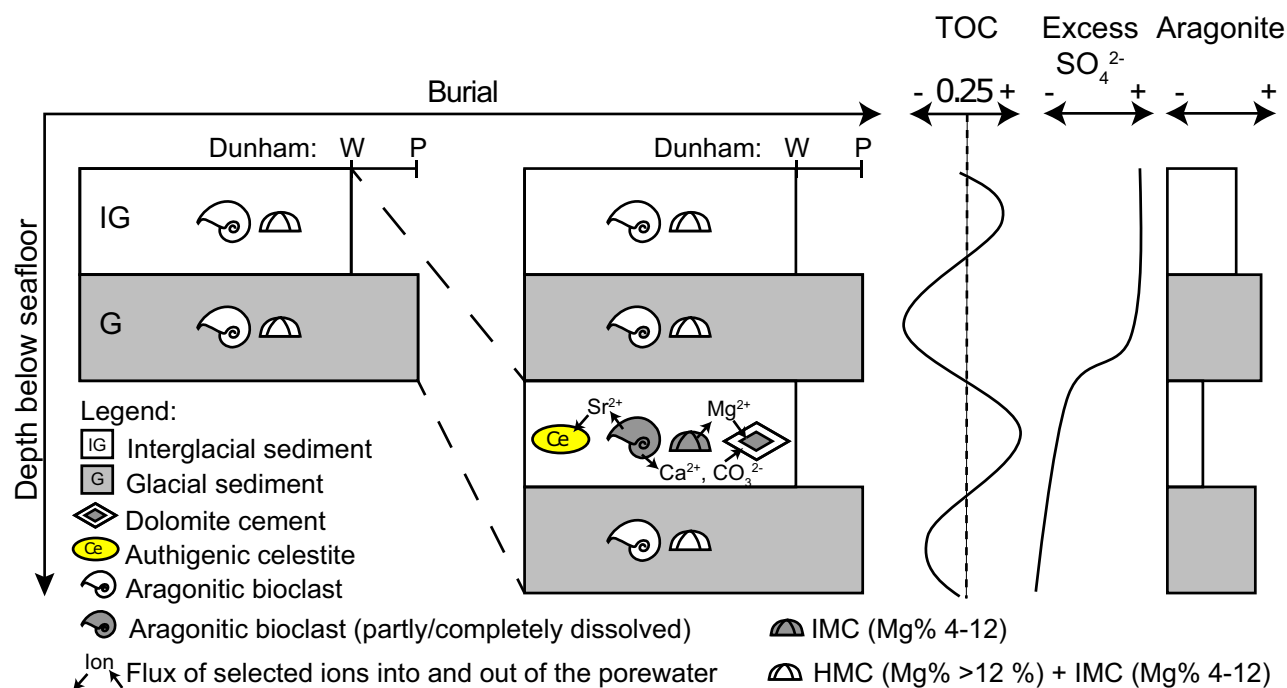


Fig. 7. Conceptual model for the dissolution of aragonite and precipitation of associated diagenetic phases.

interpreted as primary (Gerhardt *et al.*, 2000; Wall-Palmer *et al.*, 2012). However, aragonite dissolution and pteropod preservation at IODP Site U1460 are interpreted to be only indirectly coupled to glacial–interglacial cycles via more intense degradation of organic matter in interglacial intervals. This highlights the need to check for and discuss possible diagenetic influences before interpreting glacial–interglacial variability in pteropod shell preservation as a proxy for environmental change.

Bacterial sulphate reduction controlled by the availability of reactive organic matter seems to be the most important factor for aragonite dissolution and co-occurring dolomite cementation. The role of microbial processes for dolomite formation is widely discussed in the literature (Petrash *et al.*, 2017). Burdige *et al.* (2010) suggested that dolomite precipitation could be facilitated by the presence of bacterial extracellular polymeric substances (EPS). Isotope evidence suggests that dolomites, similar to the ones from this study, were formed at the margin of Great Bahama Bank in a sulphate reduction zone. However, Mg-isotope results from the same study indicate that dolomite formation was likely not mechanically dependent on the presence of sulphate reducing bacteria (Murray *et al.*, 2021). Rivers *et al.* (2019) studied the geochemistry of coastal water in Qatar, which is characterized by a wide range of salinities (40 to 340), alkalinity, pH and Mg/Ca ratios. However, active dolomitization was only observed in one sample which was influenced by sulphate reduction but was absent from many sites that showed active microbial mat growth (Rivers *et al.*, 2019). They concluded that low carbonate saturation due to anoxic breakdown of organic matter might be essential for dolomitization, rather than the presence of microbial substances. This issue cannot be resolved with our data, but the link between the aragonite dissolution proxy LDX and dolomite formation is consistent with the idea that low carbonate saturation levels might be necessary for dolomite formation. This condition might be met in microenvironments, even though the bulk porewater is still supersaturated with respect to aragonite (Fig. 6F).

At IODP Site U1460, the availability of reactive organic matter for sulphate reduction fluctuates on a metre-scale with on average increased concentrations in interglacial intervals. This provides a mechanism for the indirect coupling between dolomite formation and orbital cycles. Potentially, these initially small amounts of

dolomite could act as seeds for later, genetically unrelated dolomitization phases. This could enhance the initially relatively minor differences.

The described diagenetic processes are not limited to carbonates from temperate water. However, the initial aragonite content in tropical settings is generally higher, with, for example, *ca* 95% aragonite in the Holocene wedge on the leeward margin of Great Bahama Bank (Roth & Reijmer, 2005) compared to *ca* 70% in Holocene temperate carbonates on the southern shelf of Australia (Rivers *et al.*, 2008). The dissolution of half of the aragonite at the margin of Great Bahama Bank would reduce the measured aragonite content from 95 to 90%. The dissolution of the same amount of aragonite would reduce an initial aragonite content of 70% to 43%. In this study the bulk aragonite content is reduced from around 30% to *ca* 20% in interglacials (Fig. 3). Such a low degree of aragonite dissolution likely would have a very small effect on the total aragonite content of highly aragonitic (>70%) periplatform deposits. The same amount of aragonite dissolution therefore might be more readily recognized in the bulk mineralogy of temperate carbonates compared to tropical ones.

## CONCLUSIONS

Aragonite dissolution and incipient dolomite formation were observed in the upper 25 m below the seafloor at IODP Site U1460 on the western Australian margin. Aragonite dissolution, estimated from the Limacina Dissolution Index (LDX) is negligible at the seafloor in the outer ramp to upper slope setting, but strongly intensifies at 5 to 6 m below the seafloor. The LDX values show evidence of significant dissolution below this depth, although porewater based saturation-state calculations indicate that bulk porewater is supersaturated with respect to aragonite at all depths. Aragonite dissolution likely occurs in disseminated microenvironments, which is indicated by the very variable preservation of aragonitic pteropod shells within individual LDX samples.

Low amounts of dolomite cement (<15%) are observed to precipitate at the same depth (5 to 6 m) as aragonite dissolution intensifies. Dolomite therefore likely forms where more kinetically favourable phases of carbonate cannot precipitate. Below a depth of 5 to 6 m the dolomite formation and aragonite dissolution also show covariance on a metre-scale, with on

average higher dolomite contents and stronger aragonite dissolution in interglacial compared to glacial intervals. This differential diagenesis, which enhances primary differences in mineralogy between beds, is attributed to more intense suboxic degradation in interglacial compared to glacial intervals.

Dolomite formation and aragonite dissolution are interpreted to take place in porewaters influenced by low levels (<3 Mm) of bacterial sulphate reduction, although the low resolution of the porewater dataset does not allow to compare the intensity of this process between glacial and interglacial intervals. However, the observed incipient sulphate reduction is expected to create microenvironments undersaturated with respect to aragonite. Sulphate reduction is interpreted to be limited by the availability of reactive organic matter, since the site is from an oligotrophic setting and has a mean total organic carbon (TOC) of only *ca* 0.2%, with on average higher values in interglacial than in glacial intervals. These higher TOC values in interglacial intervals are interpreted to allow the creation of more microenvironments undersaturated with respect to aragonite. This mechanism results in an indirect coupling between dolomite formation, aragonite dissolution and orbital cycles.

## ACKNOWLEDGEMENTS

The Integrated Ocean Drilling Program (IODP) is gratefully acknowledged for providing core samples for the study. We thank three anonymous reviewers and the editor Nicholas Tosca for their detailed and helpful comments and suggestions, that improved the quality of the manuscript. The authors thank Uwe Wollenberg for his help with during SEM and EDX analysis. We acknowledge the help of Birgit Mohr with photography and image processing. SEPM is acknowledged for the permission to use parts of figures from James *et al.* (1999) for our Fig. 1. Easy Company is gratefully acknowledged for providing the EasyCore software under Academic User License agreement. This work was supported by a grant from the German Academic Scholarship Foundation (Studienstiftung des Deutschen Volkes) awarded to Hanaa Deik. Further funding was provided by the DFG (German Science Foundation, Project 320220579) to Lars Reuning. Open Access funding enabled and organized by Projekt DEAL.

## AUTHOR CONTRIBUTIONS

LR: funding acquisition, conceptualization, resources, investigation, visualization, writing – original draft, writing – review and editing. HD: funding acquisition, investigation, visualization, writing – original draft, writing – review and editing. BP and GA: investigation, writing – review and editing. HT, YI, MC, M-AB: resources, writing – review and editing.

## DATA AVAILABILITY STATEMENT

The data that supports the findings of this study are available in the Appendices S1–S6 of this article.

## REFERENCES

- Alexandersson, E.T. (1978) Destructive diagenesis of carbonate sediments in the eastern Skagerrak. *North Sea. Geol.*, **6**, 324.
- Arning, E.T., Fu, Y., van Berk, W. and Schulz, H.-M. (2011) Organic carbon remineralisation and complex, early diagenetic solid–aqueous solution–gas interactions: Case study ODP Leg 204, Site 1246 (Hydrate Ridge). *Mar. Chem.*, **126**, 120–131.
- Auderset, A., Schmitt, M. and Martínez-García, A. (2020) Simultaneous extraction and chromatographic separation of n-alkanes and alkenones from glycerol dialkyl glycerol tetraethers via selective Accelerated Solvent Extraction. *Org. Geochem.*, **143**, 103979.
- Auer, G., Petrick, B., Yoshimura, T., Mamo, B.L., Reuning, L., Takayanagi, H., De Vleeschouwer, D. and Martinez-Garcia, A. (2021) Intensified organic carbon burial on the Australian shelf after the Middle Pleistocene transition. *Quatern. Sci. Rev.*, **262**, 106965.
- Bednaršek, N., Tarling, G.A., Bakker, D.C.E., Fielding, S. and Feely, R.A. (2014) Dissolution dominating calcification process in polar pteropods close to the point of aragonite undersaturation. *PLoS One*, **9**, e109183.
- Ben-Yaakov, S. (1973) pH buffering of pore water of recent anoxic marine sediments. *Limnol. Oceanogr.*, **18**, 86–94.
- Boyer, T.P., Garcia, H.E., Locarnini, R.A., Zweng, M.M., Mishonov, A.V., Reagan, J.R., Weathers, K.A., Baranova, O.K., Paver, C.R., Seidov, D. and Smolyar, I.V. (2018) World Ocean Atlas 2018. 1° monthly averages. Dataset. <https://www.ncei.noaa.gov/archive/accession/NCEI-WOA18>. Accessed June 17, 2021.
- Brachert, T. and Dullo, W.-C. (2000) Shallow burial diagenesis of skeletal carbonates: selective loss of aragonite shell material (Miocene to Recent, Queensland Plateau and Queensland Trough, NE Australia) — implications for shallow cool-water carbonates. *Sed. Geol.*, **136**, 169–187.
- Brooke, B.P., Olley, J.M., Pietsch, T., Playford, P.E., Haines, P.W., Murray-Wallace, C.V. and Woodroffe, C.D. (2014) Chronology of Quaternary coastal aeolianite deposition and the drowned shorelines of southwestern Western Australia – a reappraisal. *Quatern. Sci. Rev.*, **93**, 106–124.



- Burdige, D.J., Hu, X. and Zimmerman, R.C. (2010) The widespread occurrence of coupled carbonate dissolution/precipitation in surface sediments on the Bahamas Bank. *Am. J. Sci.*, **310**, 492–521.
- Collins, L.B. (1988) Sediments and history of the Rottnest Shelf, southwest Australia: a swell-dominated, non-tropical carbonate margin. *Sed. Geol.*, **60**, 15–49.
- Collins, L.B., James, N.P. and Bone, Y. (2014) Chapter 19 Carbonate shelf sediments of the western continental margin of Australia. *Geol. Soc. London Mem.*, **41**(1), 255–272. <https://doi.org/10.1144/M41.19>
- De Deckker, P. (2004) On the celestite-secreting *Acantharia* and their effect on seawater strontium to calcium ratios. *Hydrobiologia*, **517**, 1–13.
- Deik, H., Reuning, L. and Pfeiffer, M. (2017) Orbital scale variation of primary productivity in the central equatorial Indian Ocean (Maldives) during the early Pliocene. *Palaeogeogr. Palaeoclimatol. Palaeoecol.*, **480**, 33–41.
- Deik, H., Reuning, L., Petrick, B. and Takayanagi, H. (2019) Hardened faecal pellets as a significant component in deep water, subtropical marine environments. *Depositional Rec.*, **5**, 348–361.
- Deik, H., Reuning, L., Courtillot, M., Petrick, B. and Bassetti, M.-A. (2021) The sedimentary record of Quaternary glacial to interglacial sea-level change on a subtropical carbonate ramp: Southwest Shelf of Australia. *Sedimentology*, **68**, 593–608.
- Dickson, A.G. and Goyet, C. (1994) *Handbook of Methods for the Analysis of the Various Parameters of the Carbon Dioxide System in Sea Water. Version 2*. United States. <https://www.osti.gov/biblio/10107773>.
- Dix, G.R. (1997) Stratigraphic patterns of deep-water dolomite, Northeast Australia. *J. Sediment. Res.*, **67**(6), 1083–1096. <https://doi.org/10.1306/D42686D0-2B26-11D7-8648000102C1865D>
- Dix, G.R. and Mullins, H.T. (1992) Shallow-burial diagenesis of deep-water carbonates, northern Bahamas: Results from deep-ocean drilling transects. *Geol. Soc. Am. Bull.*, **104**, 303–315.
- Dix, G.R. and Nelson, C.S. (2006) Diagenetic potential for lithification of cool-water carbonate shelf mud. *Sed. Geol.*, **185**, 41–58.
- Drupp, P.S., de Carlo, E.H. and Mackenzie, F.T. (2016) Porewater CO<sub>2</sub>-carbonic acid system chemistry in permeable carbonate reef sands. *Mar. Chem.*, **185**, 48–64.
- Eberli, G.P., Swart, P.K. and Malone, M.J., Eds. (1997) *Proceedings of Ocean Drilling Program Initial Reports*, 166. Ocean Drilling Program, College Station, TX.
- Gallagher, S.J., Fulthorpe, C.S., Bogus, K., Auer, G., Baranwal, S., Castañeda, I.S., Christensen, B.A., de Vleeschouwer, D., Franco, D.R., Groeneveld, J., Gurnis, M., Haller, C., He, Y., Henderiks, J., Himmler, T., Ishiwa, T., Iwatani, H., Jatinigrum, R.S., Kominz, M.A., Korpany, C.A., Lee, E.Y., Levin, E., Mamo, B.L., McGregor, H.V., McHugh, C.M., Petrick, B.F., Potts, D.C., Rastegar Lari, A., Renema, W., Reuning, L., Takayanagi, H. and Zhang, W. (2017) Expedition 356 summary. In: *Indonesian Throughflow. Proceedings of the International Ocean Discovery Program*, Vol. **356** (Eds Gallagher, S.J., Fulthorpe, C.S. and Bogus, K.), International Ocean Discovery Program, College Station, TX, 43 pp. [https://publications.iodp.org/proceedings/356/101/356\\_101.html](https://publications.iodp.org/proceedings/356/101/356_101.html).
- Gerhardt, S., Groth, H., Rühlemann, C. and Henrich, R. (2000) Aragonite preservation in late Quaternary sediment cores on the Brazilian Continental Slope: implications for intermediate water circulation. *Int. J. Earth Sci.*, **88**, 607–618.
- Gerhardt, S. and Henrich, R. (2001) Shell preservation of *Limacina inflata* (Pteropoda) in surface sediments from the Central and South Atlantic Ocean: a new proxy to determine the aragonite saturation state of water masses. *Deep Sea Res. Part I*, **48**, 2051–2071.
- Godfrey, J.S. and Ridgway, K.R. (1985) The large-scale environment of the poleward-flowing leewin current, Western Australia: longshore steric height gradients, wind stresses and geostrophic flow. *J. Phys. Oceanogr.*, **15**, 481–495.
- Groeneveld, J., Henderiks, J., Renema, W., McHugh, C.M., de Vleeschouwer, D., Christensen, B.A., Fulthorpe, C.S., Reuning, L., Gallagher, S.J., Bogus, K., Auer, G. and Ishiwa, T. (2017) Australian shelf sediments reveal shifts in Miocene Southern Hemisphere westerlies. *Sci. Adv.*, **3**, e1602567.
- Haller, C., Hallock, P., Hine, A.C. and Smith, C.G. (2018) Benthic foraminifera from the Carnarvon Ramp reveal variability in Leeuwin Current activity (Western Australia) since the Pliocene. *Mar. Micropaleontol.*, **142**, 25–39.
- Hammer, Ø., Harper, D.A.P. and Ryan, P.D. (2001) Past. Paleontological statistics software package for education and data analysis. *Palaeontol. Electron.*, **4**, 1–9.
- Hedges, J.I. and Keil, R.G. (1995) Sedimentary organic matter preservation: an assessment and speculative synthesis. *Mar. Chem.*, **49**, 81–115.
- IODP (2011) *IODP Depth Scales Terminology*. <http://www.iodp.org/policies-and-guidelines/142-iodp-depth-scales-terminology-april-2011/file>. Accessed October 28, 2021.
- James, N.P. and Bone, Y. (1989) Petrogenesis of Cenozoic, Temperate Water Calcarenes, South Australia: A Model for Meteoric/Shallow Burial Diagenesis of Shallow Water Calcite Sediments. *J. Sediment. Res.*, **59**(2), 191–203.
- James, N.P., Bone, Y. and Kyser, T.K. (2005) Where Has All the Aragonite Gone? Mineralogy of Holocene Neritic Cool-Water Carbonates, Southern Australia. *J. Sediment. Res.*, **75**, 454–463.
- James, N.P., Collins, L.B., Bone, Y. and Hallock, P. (1999) Subtropical carbonates in a temperate realm; modern sediments on the Southwest Australian shelf. *J. Sediment. Res.*, **69**, 1297–1321.
- James, N.P. and Lukasik, J.J. (2010) Cool- and cold-water carbonates. In: *Facies Models 4* (Eds James, N.P. and Dalrymple, R.W.), 4th edn, pp. 369–398. Geol. Assoc. of Canada, St. Johns.
- Krause, S., Liebetrau, V., Gorb, S., Sánchez-Román, M., McKenzie, J.A. and Treude, T. (2012) Microbial nucleation of Mg-rich dolomite in exopolymeric substances under anoxic modern seawater salinity: New insight into an old enigma. *Geology*, **40**, 587–590.
- Ku, T., Walter, L.M., Coleman, M.L., Blake, R.E. and Martini, A.M. (1999) Coupling between sulfur recycling and syndepositional carbonate dissolution: evidence from oxygen and sulfur isotope composition of pore water sulfate, South Florida Platform, U.S.A. *Geochim. Cosmochim. Acta*, **63**, 2529–2546.
- van Lith, Y., Warthmann, R., Vasconcelos, C. and McKenzie, J.A. (2003) Sulphate-reducing bacteria induce low-temperature Ca-dolomite and high Mg-calcite formation. *Geobiology*, **1**, 71–79.
- McMillan, J.D. (1982) *A Global Atlas of GEOS-3 Significant Wave Height Data and Comparison of the Data with National Buoy Data (156882)*. NASA, Wallops Flight Center, Wallops Island, VA.

- Milliman, J.D., Müller, G. and Förstner, U. (1974) *Recent Sedimentary Carbonates. Part 1 Marine Carbonates*. Springer, Berlin, Heidelberg.
- Morse, J.W. and Mackenzie, F.T. (1990) *Geochemistry of Sedimentary Carbonates*. Elsevier, Amsterdam, 707 pp.
- Murray, S.T., Higgins, J.A., Holmden, C., Lu, C. and Swart, P.K. (2021) Geochemical fingerprints of dolomitization in Bahamian carbonates: Evidence from sulphur, calcium, magnesium and clumped isotopes. *Sedimentology*, **68**, 1–29.
- Nelson, C.S. (1988) An introductory perspective on non-tropical shelf carbonates. *Sed. Geol.*, **60**, 3–12.
- Oakes, R.L. and Sessa, J.A. (2020) Determining how biotic and abiotic variables affect the shell condition and parameters of *Heliconoides inflatus* pteropods from a sediment trap in the Cariaco Basin. *Biogeosciences*, **17**, 1975–1990.
- Olsen, A., Key, R.M., van Heuven, S., Lauvset, S.K., Velo, A., Lin, X., Schirnick, C., Kozyr, A., Tanhua, T., Hoppema, M., Jutterström, S., Steinfeldt, R., Jeansson, E., Ishii, M., Pérez, F.F. and Suzuki, T. (2016) The Global Ocean Data Analysis Project version 2 (GLODAPv2) – an internally consistent data product for the world ocean. *Earth Syst. Sci. Data*, **8**, 297–323.
- Olsen, A., Lange, N., Key, R.M., Tanhua, T., Álvarez, M., Becker, S., Bittig, H.C., Carter, B.R., Da Cotrim Cunha, L., Feely, R.A., van Heuven, S., Hoppema, M., Ishii, M., Jeansson, E., Jones, S.D., Jutterström, S., Karlsen, M.K., Kozyr, A., Lauvset, S.K., Lo Monaco, C., Murata, A., Pérez, F.F., Pfeil, B., Schirnick, C., Steinfeldt, R., Suzuki, T., Telszewski, M., Tilbrook, B., Velo, A. and Wanninkhof, R. (2019) GLODAPv2.2019 – an update of GLODAPv2. *Earth Syst. Sci. Data*, **11**, 1437–1461.
- Parkhurst, D.L. and Appelo, C. (2013) *Description of Input and Examples for PHREEQC Version 3: A Computer Program for Speciation, Batch-Reaction, One-Dimensional Transport, and Inverse Geochemical Calculations*. 6-A43, Reston, VA, 519 pp.
- Pettrash, D.A., Bialik, O.M., Bontognali, T.R., Vasconcelos, C., Roberts, J.A., McKenzie, J.A. and Konhauser, K.O. (2017) Microbially catalyzed dolomite formation: From near-surface to burial. *Earth Sci. Rev.*, **171**, 558–582.
- Petrack, B., Martínez-García, A., Auer, G., Reuning, L., Auderset, A., Deik, H., Takayanagi, H., de Vleeschouwer, D., Iryu, Y. and Haug, G.H. (2019a) Glacial Indonesian Throughflow weakening across the Mid-Pleistocene Climatic Transition. *Sci. Rep.*, **9**, 16995.
- Petrack, B., McClymont, E.L., Felder, S., Rueda, G., Leng, M.J. and Rosell-Melé, A. (2015) Late Pliocene upwelling in the Southern Benguela region. *Palaeogeogr. Palaeoclimatol. Palaeoecol.*, **429**, 62–71.
- Petrack, B., McClymont, E.L., Littler, K., Rosell-Melé, A., Clarkson, M.O., Maslin, M., Röhl, U., Shevenell, A.E. and Pancost, R.D. (2018) Oceanographic and climatic evolution of the southeastern subtropical Atlantic over the last 3.5 Ma. *Earth Planet. Sci. Lett.*, **492**, 12–21.
- Petrack, B., Reuning, L. and Martínez-García, A. (2019b) Distribution of glycerol dialkyl glycerol tetraethers (GDGTs) in microbial mats from Holocene and Miocene sabkha sediments. *Front Earth Sci.*, **7**, 310. <https://doi.org/10.3389/feart.2019.00310>
- Plummer, N., Parkhurst, D.L., Fleming, G.W. and Dunkle, S.A. (1988) A computer program incorporating Pitzer's equations for calculation of geochemical reactions in brines. 88-4153.
- Porter-Smith, R., Harris, P.T., Andersen, O.B., Coleman, R., Greenslade, D. and Jenkins, C.J. (2004) Classification of the Australian continental shelf based on predicted sediment threshold exceedance from tidal currents and swell waves. *Mar. Geol.*, **211**, 1–20.
- Reuning, L., Reijmer, J. and Betzler, C. (2002) Sedimentation cycles and their diagenesis on the slope of a Miocene carbonate ramp (Bahamas, ODP Leg 166). *Mar. Geol.*, **185**, 121–142.
- Reuning, L., Reijmer, J. and Mattioli, E. (2006) Aragonite cycles: diagenesis caught in the act. *Sedimentology*, **53**, 849–866.
- Rivers, J.M., James, N.P. and Kyser, T.K. (2008) Early diagenesis of carbonates on a cool-water carbonate shelf, southern Australia. *J. Sediment. Res.*, **78**, 784–802.
- Rivers, J.M., Kyser, T.K. and James, N.P. (2012) Salinity reflux and dolomitization of southern Australian slope sediments: the importance of low carbonate saturation levels. *Sedimentology*, **59**, 445–465.
- Rivers, J.M., Varghese, L., Yousif, R., Whitaker, F.F., Skeat, S.L. and Al-Shaikh, I. (2019) The Geochemistry of Qatar Coastal Waters and its Impact on Carbonate Sediment Chemistry and Early Marine Diagenesis. *J. Sediment. Res.*, **89**, 293–309.
- Rivers, J.M., Yousif, R., Kaczmarek, S.E. and Al-Shaikh, I. (2021) Cenozoic coastal carbonate deposits of Qatar: Evidence for dolomite preservation bias in highly-arid systems. *Sedimentology*, **68**, 771–787.
- Roth, S. and Reijmer, J. (2005) Holocene millennial to centennial carbonate cyclicity recorded in slope sediments of the Great Bahama Bank and its climatic implications. *Sedimentology*, **52**, 161–181.
- Sabine, C.L., Key, R.M., Feely, R.A. and Greeley, D. (2002) Inorganic carbon in the Indian Ocean: Distribution and dissolution processes. *Global Biogeochem. Cycles*, **16**, 15–15-18.
- Salacup, J.M., Farmer, J.R., Herbert, T.D. and Prell, W.L. (2019) Alkenone Paleothermometry in Coastal Settings: Evaluating the Potential for Highly Resolved Time Series of Sea Surface Temperature. *Paleoceanogr. Paleoclimatol.*, **34**, 164–181.
- Sanders, D. (2003) Syndepositional dissolution of calcium carbonate in neritic carbonate environments: geological recognition, processes, potential significance. *J. Afr. Earth Sci.*, **36**, 99–134.
- Saxena, S. and Betzler, C. (2003) Genetic sequence stratigraphy of cool water slope carbonates (Pleistocene Eucla Shelf, southern Australia). *Int. J. Earth Sci.*, **92**, 482–493.
- Schulte, S. and Bard, E. (2003) Past changes in biologically mediated dissolution of calcite above the chemical lysocline recorded in Indian Ocean sediments. *Quatern. Sci. Rev.*, **22**, 1757–1770.
- Smith, A.M. and Nelson, C.S. (2003) Effects of early sea-floor processes on the taphonomy of temperate shelf skeletal carbonate deposits. *Earth Sci. Rev.*, **63**, 1–31.
- Spooner, M.I., de Deckker, P., Barrows, T.T. and Fifield, L.K. (2011) The behaviour of the Leeuwin Current offshore NW Australia during the last five glacial–interglacial cycles. *Global Planet. Change*, **75**, 119–132.
- Sreevidya, E., Sijinkumar, A.V. and Nath, B.N. (2019) Aragonite pteropod abundance and preservation records from the Maldives, equatorial Indian Ocean: Inferences on past oceanic carbonate saturation and dissolution events. *Palaeogeogr. Palaeoclimatol. Palaeoecol.*, **534**, 109313.
- Swart, P.K. (1993) The Formation of Dolomite in Sediments from the Continental Margin of Northeastern Queensland. In: *Proceedings of the Ocean Drilling Program*, 133

- Scientific Results* (Eds McKenzie, J.A., Davies, P.J. and Palmer-Julson, A.). pp. 513–523. Ocean Drilling Program, College Station, TX.
- Swart, P.K. and Guzikowski, M.** (1988) Interstitial-Water Chemistry and Diagenesis of Periplatform Sediments from the Bahamas, ODP Leg 101. In: *Proceedings of the Ocean Drilling Program, 101 Scientific Results* (Eds Austin Jr, J.A. and Schlager, W.), pp. 363–380. Ocean Drilling Program, College Station, TX.
- Swart, P.K. and Melim, L.A.** (2000) The Origin of Dolomites in Tertiary Sediments from the Margin of Great Bahama Bank. *J. Sediment. Res.*, **70**, 738–748.
- Volkman, J.K., Barrett, S.M., Blackburn, S.I., Mansour, M.P., Sikes, E.L. and Gelin, F.** (1998) Microalgal biomarkers: A review of recent research developments. *Org. Geochem.*, **29**, 1163–1179.
- Wall-Palmer, D., Hart, M.B., Smart, C.W., Sparks, R.S.J., Le Friant, A., Boudon, G., Deplus, C. and Komorowski, J.C.** (2012) Pteropods from the Caribbean Sea: variations in calcification as an indicator of past ocean carbonate saturation. *Biogeosciences*, **9**, 309–315.
- Wall-Palmer, D., Smart, C.W. and Hart, M.B.** (2013) In-life pteropod shell dissolution as an indicator of past ocean carbonate saturation. *Quatern. Sci. Rev.*, **81**, 29–34.
- Walter, L.M. and Burton, E.A.** (1990) Dissolution of Recent platform carbonate sediments in marine pore fluids. *Am. J. Sci.*, **290**, 601–643.
- Walter, L.M. and Morse, J.W.** (1984) Magnesian calcite stabilities: A reevaluation. *Geochim. Cosmochim. Acta*, **48**, 1059–1069.
- Walter, L.M. and Morse, J.W.** (1985) The dissolution kinetics of shallow marine carbonates in seawater: A laboratory study. *Geochim. Cosmochim. Acta*, **49**, 1503–1513.
- Wright, D.T. and Wacey, D.** (2005) Precipitation of dolomite using sulphate-reducing bacteria from the Coorong Region, South Australia: significance and implications. *Sedimentology*, **52**, 987–1008.
- Wright, P. and Cherns, L.** (2004) Are there "black holes" in carbonate deposystems? *Geologica Acta*, **2004**, 285–290.
- Zhang, F., Xu, H., Konishi, H., Kemp, J.M., Roden, E.E. and Shen, Z.** (2012) Dissolved sulfide-catalyzed precipitation of disordered dolomite: Implications for the formation mechanism of sedimentary dolomite. *Geochim. Cosmochim. Acta*, **97**, 148–165.

*Manuscript received 16 December 2020; revision accepted 1 February 2022*

## Supporting Information

Additional information may be found in the online version of this article:

**Appendix S1.** Cross-plots of carbonate mineral phrases, total organic carbon (TOC) and alkenone concentrations.

**Appendix S2.** Table of X-ray diffraction (XRD)-derived mineralogy.

**Appendix S3.** Table of alkenone concentrations.

**Appendix S4.** Table of grain-size fraction >63 µm.

**Appendix S5.** Table of the average Limacena Dissolution Index (LDX).

**Appendix S6.** Table of total organic carbon (TOC) values.